Available online at www.sciencedirect.com
ScienceDirect
Acta Materialia 56 (2008) 5544–5551
Acta MATERIALIA
www.elsevier.com/locate/actamat

Coarsening kinetics of γ' precipitates in the Ni–Al–Mo system

Tao Wang [a,*], Guang Sheng [b], Zi-Kui Liu [b], Long-Qing Chen [b]

[a] Department of Materials Science and Engineering, Iowa State University, 2220 Hoover Hall, Ames, IA 50011, USA
[b] Department of Materials Science and Engineering, The Pennsylvania State University, University Park, PA 16802, USA

Received 10 April 2008; received in revised form 8 July 2008; accepted 22 July 2008
Available online 20 August 2008

Abstract

The effect of Mo on the microstructure evolution and coarsening kinetics of γ' precipitates in the Ni–Al–Mo system is studied using phase-field simulations with inputs from thermodynamic, kinetic and lattice parameter databases. For alloys of different compositions, the precipitate morphology and the statistical information of precipitate sizes are predicted as a function of annealing time. It is observed that increasing Mo content leads to a change of the precipitate morphology from being cuboidal to spherical as well as a reduction in the coarsening rate. Comparison between simulated results and existing experimental microstructure morphologies and coarsening rates shows good agreements.

Keywords: Ni-base superalloys; Phase-field simulation; Morphology; Coarsening kinetics

1. Introduction

A typical microstructure of Ni-base superalloys contains $L1_2$-ordered γ' precipitate particles coherently embedded in a face-centered cubic (fcc, γ) matrix. The mechanical properties of a Ni-base superalloy depend on the volume fraction and morphology of γ' precipitates. With sufficient thermal energy, γ' precipitates undergo coarsening, also called Ostwald ripening, during which smaller particles dissolve and larger particles grow. This may occur at later stages in the precipitation process or during service at high temperatures. Thus a knowledge of the coarsening process of γ' precipitates is essential for the design and application of Ni-base superalloys. As one of the commonly used alloy elements in Ni-base superalloys, Mo has been shown to modify both the morphology and coarsening rate of γ' precipitates [1–4]. The main purpose of this work is to develop a phase-field model for ternary Ni-base alloys based on earlier works on the Ni–Al binary system [5–9], and apply it to study the morphological evolution and coarsening kinetics of γ' precipitates in the Ni–Al–Mo ternary system through two-dimensional (2-D) simulations. The effect of precipitate volume fraction on the coarsening kinetics is also discussed.

2. Simulation details

2.1. Model

In recent years, phase-field simulations have been widely used to study various phenomena in Ni alloys, including solidification [10,11], nucleation and growth [12–15], phase transformation [16–18], multicomponent diffusion [19,20], bimodal particle size distribution [21], rafting [22] and coarsening [5–9,23]. In a phase-field model, all phases or domains in a microstructure are characterized by a set of field variables, e.g. compositions and order parameters. These field variables are continuous across the interface regions. The order parameters can be the physical long-range order parameters of the $L1_2$-ordered phase [8] or artificial phase fields [7,9]. In this work, we chose the later, which, although physically less appealing, allows simulations at larger length scales. To distinguish the disordered γ phase and the ordered

* Corresponding author.
E-mail address: taowang@iastate.edu (T. Wang).

1359-6454/$34.00
doi:10.1016/j.actamat.2008.07.024

γ' phase with four types of ordered domains in Ni–Al–Mo ternary alloys, two composition variables $c_i(\mathbf{r}, t)(i = \text{Al, Mo})$ and four artificial order parameters $\eta_j(\mathbf{r}, t)(j = 1, 2, 3, 4)$ are employed, which vary spatially (**r**) and temporally (t). The temporal evolution of these field variables is described by the Cahn–Hilliard and Allen–Cahn (or time-dependent Ginzburg–Laudau) equations [24]:

$$\frac{\partial c_i(\mathbf{r},t)}{\partial t} = \nabla\left[M_{im}\nabla\frac{\delta F}{\delta c_m(\mathbf{r},t)}\right], \tag{1}$$

$$\frac{\partial \eta_j(\mathbf{r},t)}{\partial t} = -L_{jn}\frac{\delta F}{\delta \eta_n(\mathbf{r},t)}, \tag{2}$$

where F is the total free energy of the microstructure including both chemical and elastic free energies, M_{im} is the diffusion mobility of species i with respect to the concentration gradient of element m, and L_{jn} is the kinetic coefficient for the relaxation of order parameter j with respect to the gradient of order parameter n.

The total chemical free energy of an inhomogeneous microstructure can be described by the field variables as [7]:

$$F = \int_v \left[f(c_i,\eta_j) + \sum_{j=1}^{4}\frac{\beta_j}{2}(\nabla\eta_j)^2\right]\mathrm{d}V, \tag{3}$$

where β_j is the gradient energy coefficient of the order parameter η_j, and $f(c_i, \eta_j)$ denotes the local free energy density of the system expressed by [25]:

$$f(c_i,\eta_j) = h(\eta_j)f^p(c_i^p) + [1-h(\eta_j)]f^m(c_i^m) + wg(\eta_j) + \mathrm{e}^{\mathrm{el}}, \tag{4}$$

where e^{el} is the elastic energy density, and w is the double-well potential height. The chemical free energy densities of the precipitate and the matrix, f^p and f^m, are obtained from the Ni–Al–Mo thermodynamic database [26]. The double-well potential $g(\eta_j)$ and the separation function $h(\eta_j)$ are selected as [7]:

$$g(\eta_j) = \sum_{j=1}^{4}[\eta_j^2(1-\eta_j)^2], \tag{5}$$

$$h(\eta_j) = \sum_{j=1}^{4}[\eta_j^3(6\eta_j^2 - 15\eta_j + 10)] \tag{6}$$

In this approach, the interface region is treated as a mixture of the γ matrix and the γ' precipitate with different compositions but equal chemical driving forces [9,25,27]:

$$\begin{cases}\dfrac{\partial f^p(c_i^p)}{\partial c_i^p} = \dfrac{\partial f^m(c_i^m)}{\partial c_i^m} \\ c_i = h(\eta_j)c_i^p + [1-h(\eta_j)]c_i^m\end{cases} \tag{7}$$

The elastic energy contribution arises from the lattice misfit between the γ and γ' phases. Assuming that the lattice parameter is a weighted average of the lattice parameters of the γ and γ' phases with $h(\eta_j)$ as the weighing factor, the local stress-free strain ε_{kl}^0 is given by [28]:

$$\varepsilon_{kl}^0 = \varepsilon_0\delta_{kl}h(\eta_j), \tag{8}$$

where ε_0 is the stress-free lattice misfit, and δ_{kl} is the Kronecker delta function. If there is no macroscopic change in shape or volume, the elastic strain $\varepsilon_{kl}^{\mathrm{el}}$ can be written as:

$$\varepsilon_{kl}^{\mathrm{el}} = \delta\varepsilon_{kl} - \varepsilon_{kl}^0, \tag{9}$$

where $\delta\varepsilon_{kl}=0.5(\partial u_k/\partial r_l+\partial u_l/\partial r_k)$ is the local strain. The vector **u** represents the local displacement field, which can be solved by using Hooke's law ($\sigma_{ij} = C_{ijkl}\varepsilon_{kl}^{\mathrm{el}}$, where C_{ijkl} refers to the elastic constants), the local mechanical equilibrium condition ($\partial\sigma_{ij}/\partial r_j = 0$), and Eqs. (8) and (9). After the displacement field is obtained, the elastic strain and stress can be determined. The elastic energy density e^{el} is given by:

$$e^{el} = \frac{1}{2}\sigma_{kl}\varepsilon_{kl}^{\mathrm{el}}. \tag{10}$$

The diffusion mobility M_{im} in the Cahn–Hilliard equation (Eq. (1)) is expressed by the following equation:

$$M_{im} = \sum_{j=1}^{n}[\delta_{mj} - c_m][\delta_{ji} - c_i]c_jM_j, \tag{11}$$

where M_j is the atomic mobility of element j from the atomic mobility database of the Ni–Al–Mo system [29]. The kinetic coefficient L in the Allen–Cahn equation (Eq. (2)) is related to the interface mobility, which is not well determined due to the lack of experimental data. However, an accurate value of L is not necessary for a diffusion-controlled process [7], and a constant value for L is thus assigned. By comparing the simulated results of different L values, we used $L = 0.001\ \mathrm{ms^{-1}\,J^{-1}}$ in this work because a larger L will not change the results, which means $0.001\ \mathrm{ms^{-1}\,J^{-1}}$ is large enough to ensure a diffusion-controlled process.

2.2. Conditions and parameters for simulations

In order to compare with experimental results [3], phase-field simulations at a temperature of 1048 K were performed using a 512×512 grid with a unit grid size of 2 nm. Three alloys with different Mo compositions were selected for simulations and their overall compositions are shown in Fig. 1 as solid circles. The dashed lines in Fig. 1 are the tie-lines for the three alloys calculated from the thermodynamic database [26]. More alloys with different volume fractions of precipitates are selected along the tie-lines (open symbols in Fig. 1). The initial states were homogeneous solutions with small composition fluctuations around the average compositions. West and Kirkwood [30] observed that the maximum precipitate density (about $10^{23}\ \mathrm{m^{-3}}$) of γ' precipitates was reached in few seconds in Ni–Al alloys at 1063 K. Consequently, approximate 1800 nuclei were introduced at an early stage of simulations ($t < 10$ s), and after that the nucleation process was turned off. All nuclei were circles with an average radius of 6 nm and randomly distributed.

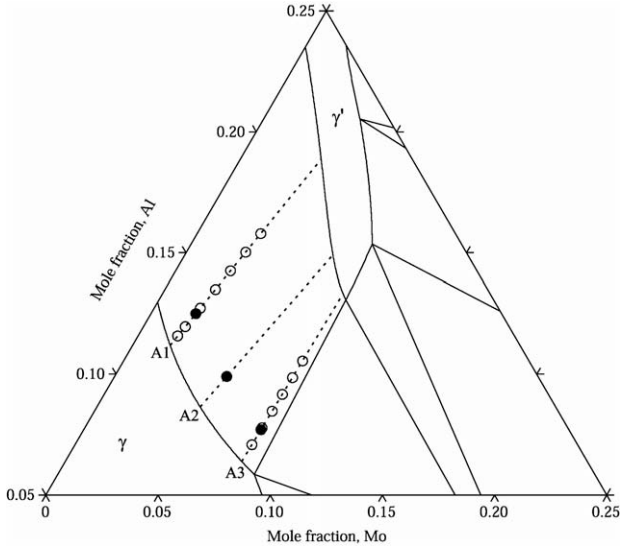

Fig. 1. Isothermal section of the Ni–Al–Mo ternary phase diagram at 1048 K. Symbols show the compositions of selected samples and dotted lines are the tie-lines for those compositions.

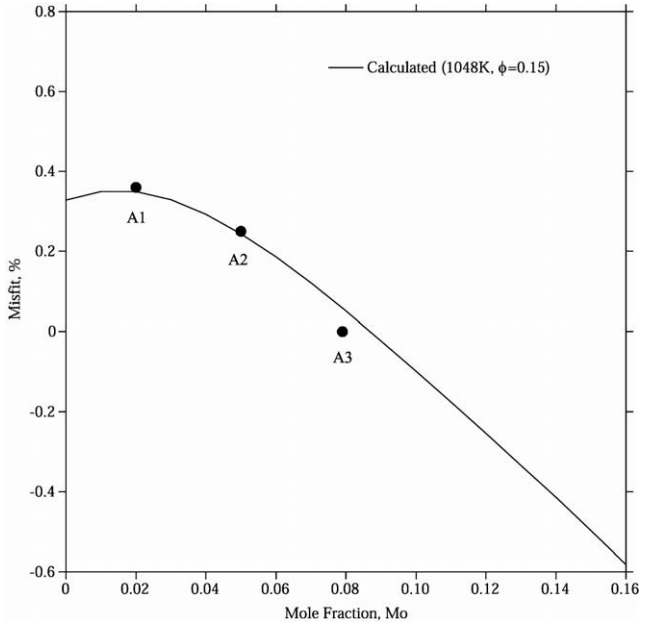

Fig. 2. Lattice misfit between γ and γ' in Ni–Al–Mo ternary system at 1048 K. Symbols show the values for A1, A2 and A3 alloys.

One of the critical factors controlling the morphology of coherent γ' precipitates is the magnitude and sign of the stress-free lattice misfit between γ and γ', which is very sensitive to the details of experimental processing [31]. We recently proposed an integrated computational approach for evaluating the lattice misfit between γ and γ' in Ni-base superalloys by combining first-principles calculations, existing experimental data and phenomenological modeling [32], and the values for the current simulations are shown in Fig. 2.

The interfacial energy is another essential parameter for the phase-field simulations. Due to the lack of data, a value of 13.5 mJ m^{-2} from binary Ni–Al alloys [33] was used in the present work, in line with the value of 12 mJ m^{-2} for superalloy Nimonic 80a (Ni–Cr–Al–Ti) reported by Zickel et al. [34]. By fitting to the interfacial energy, the gradient energy coefficients β_j and the double-well potential height w can be determined for a given interface width. Since the microstructure is described by artificial order parameters η_j in this model, a wider interface thickness than the actual physical one can be used in order to consider the large length and time scales in simulations comparable to those in experiments [7]. With an interface width of 5 nm, β_j and w are 9.0×10^{-11} J m^{-1} and 3.5×10^{7} J m^{-3}, respectively.

The temperature and composition dependences of the elastic constants of γ and γ' in Ni–Al binary alloys were studied by Prikhodko and his co-workers [35,36], though only a few Ni–Al–Mo samples were measured in a very narrow temperature range [37,38]. The elastic constants for current alloys were estimated from the above information and listed in Table 1. Furthermore, the elastic homogeneity was assumed due to the lack of data and the small difference between the γ and γ' elastic constants [7].

3. Results and discussions

3.1. Microstructure evolution

The 2-D microstructures at different annealing times are shown in Fig. 3 together with the experimental micrographs after 67 h [3]. The precipitate sizes from simulations are somewhat smaller than those from experiments. One of the reasons could be due to the 2-D nature of simulations since the coarsening in two dimensions is slower than that in three dimensions because of the reduced curvature. As shown in Fig. 3, the simulated particle morphology is very similar to the experimental observations for all three alloys. From A1 to A3, the magnitude of the lattice misfit decreases with the increase in the Mo concentration (see Fig. 2), resulting in more circular morphology due to the smaller elastic energy contributions. For A1 and A2 alloys

Table 1
Some parameters for phase-field simulations ($T = 1048$ K)

Alloy	ε_0(%)	C_{11} (GPa)	C_{12} (GPa)	C_{44} (GPa)	D^{m}_{AlAl} (m^2 s^{-1})* ($\times 10^{-17}$)	D^{m}_{MoMo} (m^2 s^{-1})* ($\times 10^{-18}$)
A1	0.36	213	151	99	2.232	2.446
A2	0.25	218	153	100	1.655	1.460
A3	0.00	217	151	98	1.263	0.826

* Calculated from the atomic mobility database [29] at the equilibrium compositions of the γ matrix.

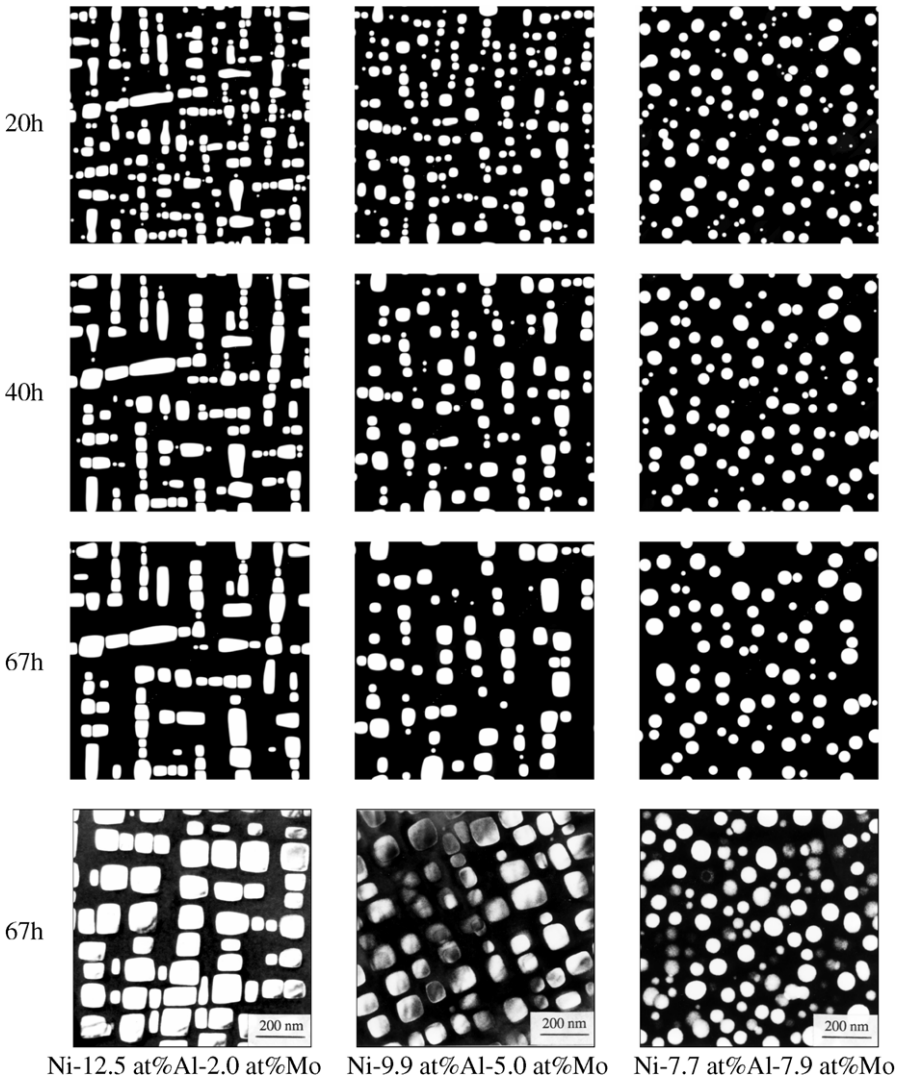

Fig. 3. Microstructure evolution of the γ' precipitates in Ni–Al–Mo alloys at 1048 K. Figures in the bottom row are from experiments [3], and others from the present 2-D phase-field simulations.

with larger lattice misfits, the γ' particles gradually change their shape from circular to rectangular with annealing time, while the particles in A3 with a smaller misfit remain circular. For all three alloys, coalescence is observed between neighboring domains described by the same order parameter, and such a phenomenon was also reported from the previous phase-field simulations in Ni–Al alloys [7]. The particle alignment along the <10> direction of the γ matrix is also found in Fig. 3, and the degree of alignment is dependent on the misfit strain. After 67 h of annealing, the γ' precipitates in A1 alloy ($\varepsilon_0 = 0.0036$) is clearly aligned, and the degree of alignment in A2 alloy ($\varepsilon_0 = 0.0025$) is relatively lower.

3.2. Coarsening kinetics

In a coarsening process, the average particle radius $\bar{R}$ obeys a temporal law, $\bar{R}^n \propto t$. The temporal dependence n changes according to the coarsening mechanism. A value of 3 is derived from the matrix-diffusion-controlled coarsening process [39,40], while interfacial-diffusion-controlled coarsening leads to $n = 4$ [41]. It is generally believed that the coarsening process of γ' precipitates in Ni-base alloys is controlled by diffusion in the matrix [7,42].

The theory developed by Lifshitz and Slyozov [39] and Wagner [40] (LSW) is often used to describe a matrix-diffusion-controlled coarsening process, according to which the average particle radius $\bar{R}$ obeys the following temporal power law:

$$\bar{R}^3 - \bar{R}_s^3 = K(t - t_s) \tag{12}$$

where K is the coarsening rate constant, and $\bar{R}_s$ and t_s refer to the average particle size and the time at the beginning of the steady-state coarsening, respectively. To avoid the ambiguity in determining the exact onset of the steady-state coarsening, Eq. (12) can be rewritten as:

$$\bar{R}^3 = \bar{R}_0^3 + Kt, \tag{13}$$

where $\bar{R}_0^3 = \bar{R}_s^3 - Kt_s$ [7]. Even though the LSW theory was derived based on the assumptions that the particles were

spherical and the volume fraction was zero, existing computer simulations as well as many of the experimental measurements [3,43] suggest that the average precipitate size as a function of time follows a cubic law in systems with non-spherical particles and in the presence of elastic interactions.

The coarsening rate constant K is described, under LSW theory, as a function of the interfacial energy, σ, the diffusion coefficient in the matrix phase, D_{ij}^m, and the second derivative of the free energy of the matrix phase with respect to the concentration in the matrix, $f_{ij}^m (= \partial^2 f^m / \partial c_i^m \partial c_j^m)$. Many efforts [44–49] has been made to study coarsening in multicomponent systems under different conditions. Kuehmann and Voorhees [45] derived the coarsening rate constant for ternary alloys by assuming a diagonal diffusivity matrix:

$$K = \frac{8\sigma V^p}{9\left(\dfrac{\Delta c_2(\Delta c_2 f_{22}^m + \Delta c_3 f_{23}^m)}{D_{22}^m} + \dfrac{\Delta c_3(\Delta c_2 f_{23}^m + \Delta c_3 f_{33}^m)}{D_{33}^m}\right)}, \tag{14}$$

where V^p is the molar volume of the precipitate phase, and Δc_i $(=c^{p,\mathrm{eq}} - c^{m,\mathrm{eq}})$ is the composition difference between the matrix and the precipitate at the equilibrium conditions. The subscripts 2 and 3 indicate the second and third components in the ternary system, i.e. Al and Mo for the current case, respectively.

A different coarsening mechanism was recently suggested by Ardell and Ozolins [50] for γ' precipitates in Ni-base alloys. According to their Monte Carlo simulations in Ni–Al alloys, Ardell and Ozolins [50] found a wide interface (~5 nm) with a ragged structure between γ and γ'. They believed that coarsening of γ' in Ni–Al alloys is controlled by diffusion in the interface, especially at the early stages when the particle size is relatively small, and then they suggested a square law (i.e. $n = 2$) for the average particle radius. Several investigations have been performed since then to determine the growth exponent n. Seidman et al. [51] studied γ' coarsening in Ni–5.2 at.% Al–14.2 at.% Cr at 873 K by 3-D atom probe tomography (APT) and reported a value of 3.33 ± 0.45 for n. The temporal behavior of the γ matrix supersaturations also supported a cubic law for coarsening. Dwarapureddy et al. [52] investigated the growth of γ' precipitates in the superalloy IN738LC, and verified that the growth exponent n was close to 3. The diffusion across the interface was taken into account in the present model by assuming an order-parameter-dependent atomic mobility of element i:

$$M_i = h(\eta_j) M_i^p + [1 - h(\eta_j)] M_i^m, \tag{15}$$

where M_i^p and M_i^m are composition-dependent atomic mobilities in the precipitate and the matrix, and the compositions are determined by Eq. (7). According to the atomic mobility database of the Ni–Al–Mo system [29], the mobility in the precipitate is about one order of magnitude smaller than that in the matrix. The effect of large mobility disparity between the matrix and the precipitate on coarsening kinetics was recently studied using phase-field simulations [53]. The mobility in the precipitate M_i^p was artificially set to be $0.1\, M_i^m$, $0.01\, M_i^m$ and 0 in order to generate enough mobility disparity between matrix and precipitates. The preliminary results indicate a coarsening time exponent n of 3.3–3.4 by non-linear fitting, which is somewhat higher than Ardell and Ozolins' prediction [50] ($n = 2$–3). One reason for this discrepancy could be the different treatments of diffusion coefficient variation across the interface. Ardell and Ozolins [50] assumed that it is a constant value across the whole interface region and 1–2 orders of magnitude slower than the diffusion mobility in the matrix, while the mobility in our simulations is described as a function of order parameters and monotonically decreases from M_i^m in the matrix to M_i^p in the precipitate. However, further studies are required to fully resolve the discrepancy.

For the coarsening of γ' precipitates in Ni–Al–Mo alloys, a cubic relationship ($\bar{R}^3 \propto t$) was reported in the literature and the coarsening rate constants were determined from experimental data [3,4]. To compare with those experimental results, the cubic law (Eq. (13)) was used in the data analysis of the present work. The relationship between the average particle size and annealing time at 1048 K from the present simulations is plotted in Fig. 4. The average particle sizes at different annealing times were obtained by following the same procedures used in the experiments [3,4]. To compare the particle coarsening rates for different alloys of different particle shapes, the radius of an area-equivalent circle was assigned to each particle. In order to obtain accurate values for the average particle size $\bar{R}$, three independent runs of simulations were performed for

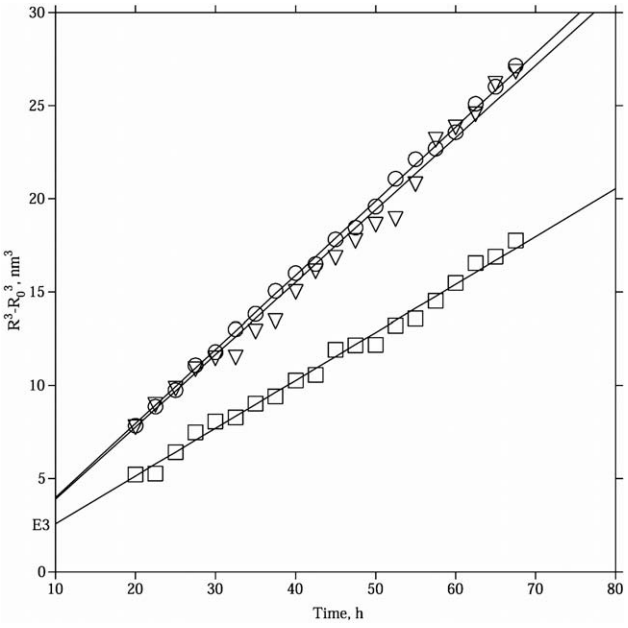

Fig. 4. Plot of the cube of average particle size vs. annealing time at 1048 K. (○: Ni–12.5 at.% Al–2.0 at.% Mo, $K = 397$ nm^3 h^{-1};▽: Ni–9.9 at.% Al–5.0 at.% Mo, $K = 388$ nm^3 h^{-1};□: Ni–7.7 at.% Al–7.9 at.% Mo, $K = 257$ nm^3 h^{-1}).

each alloy. The approximately linear relationships between $\bar{R}^3$ and t are observed for all three alloys, and the coarsening constants K were obtained from a linear regression procedure using Eq. (13).

The coarsening rate constants from the simulations at 1048 K are compared with the experimental values [3] in Fig. 5. Note that the experimental results from Ref. [4] are for 1023 K. As can be seen, both simulated and experimental coarsening rate constants decrease with the increase in Mo concentration. One reason for this phenomenon may be the reduced diffusivity (see Table 1). The coarsening rate constants from simulations are somewhat smaller than those from experiments. As mentioned before, the coarsening in two dimensions is expected to be slower than that in three dimensions because of the reduced curvature. The difference between simulations and experiments (about 300 $nm^3\ h^{-1}$ for our cases: see Fig. 5) is not very significant since as shown in Fig. 5 a temperature variation from 1048 to 1023 K could bring a change of that magnitude in the coarsening rate constants.

Since the LSW theory was developed by solving the diffusion equation for a particle in an infinite matrix, and did not consider the interactions between different particles, it can only be strictly applied to the case of zero volume fraction of the precipitate. It was reported [54–61] that the volume fraction did not affect the cubic law of coarsening but will change the value of coarsening rate constant and the shape of particle size distribution curve. Thus the coarsening rate constant K is modified to be a function of the volume fraction of particles, ϕ [62]:

$$K = K_{\mathrm{LSW}} f(\phi), \tag{16}$$

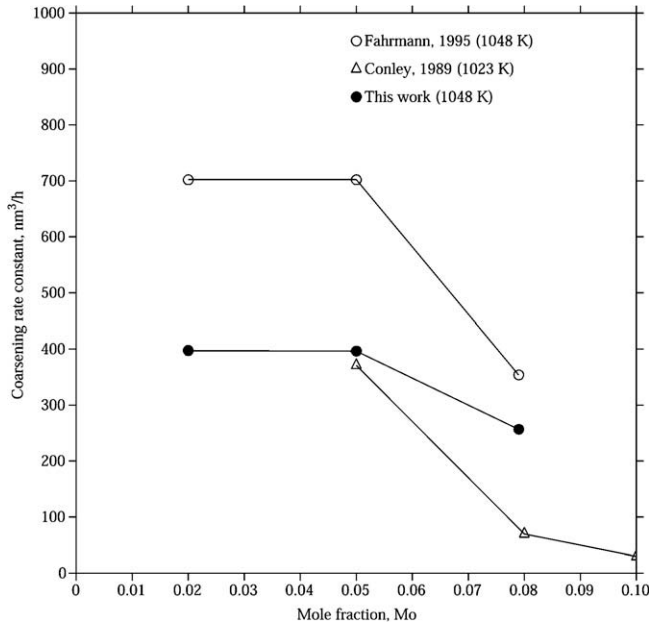

Fig. 5. Coarsening rate constant vs. Mo concentration at 1048 K. Open symbols are from experiments (○ [3]: Ni–12.5 at.% Al–2.0 at.% Mo, Ni–9.9 at.% Al–5.0 at.% Mo and Ni–7.7 at.% Al–7.9 at.% Mo; Δ [4]: Ni–10.2 at.% Al–5.1 at.% Mo, Ni–8.2 at.% Al–7.9 at.% Mo and Ni–6.5 at.% Al–9.8 at.% Mo) and solid ones from current 2-D phase-field simulations.

The contributions of the volume fraction are given by a function $f(\phi)$, which equals 1 for the zero volume fraction in line with the LSW theory. The accurate theoretical prediction of the volume fraction dependence has proved difficult [50]. Several predictions of $f(\phi)$ based on different assumptions can be found in the literature [54–57,59], predicting quite different behaviors for $f(\phi)$. These predictions have two things in common: (i) $f(\phi)$ is a monotone increasing function of ϕ; and (ii) $f(\phi)$ is independent of the alloy system.

Phase-field simulations were performed for alloys with different volume fractions of precipitates. The alloys are selected from A1 and A3 tie-lines (open symbols in Fig. 1), and the results are shown in Fig. 6. As predicted by various theories [54–57,59], the coarsening rate constant was observed to increase as the volume fraction of precipitates increases due to the reduced diffusion distance. As shown in Fig. 6, the growth of the coarsening rate constant is sluggish in the low volume fraction range, and increases in the high volume fraction range. Such a trend is best reproduced by theories provided by Asimov [54], Davies et al. [57] and Voorhees and Glicksman [59]. The anomalous dependence for small volume fractions (i.e. decreasing rather than increasing with volume fraction) reported by Ardell and co-workers in Ni–Al and Ni–Ti alloys [63] is not found in the present work.

Fig. 6 also indicates that the coarsening rate constants for A3 alloys have a stronger dependence on volume fraction than those for A1 alloys, which suggests an alloy-dependent function for $f(\phi)$. For volume fractions less than 0.3, coarsening for A3 alloys is slower than that for A1 alloys, while A3 alloys have a higher coarsening rate than A1 alloys when the volume fraction is over 0.4. This obser-

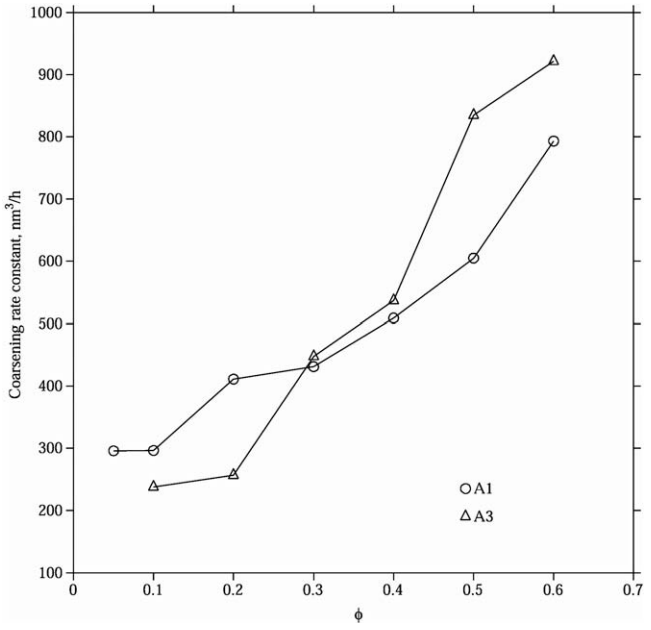

Fig. 6. Coarsening rate constant vs. volume fraction of γ' precipitates in the Ni–Al–Mo system at 1048 K.

vation may be explained by the particle shape variations. It is well known that the coarsening process is driven by the variation in interfacial curvature and realized by mass diffusion through the matrix. A1 alloys have high diffusivities and low curvatures (low driving forces) due to the rectangular particle shape, while A3 alloys have low diffusivities and high curvatures (high driving forces) because their particles are circular. When the volume fraction of precipitates is low, the diffusion distance is long and the coarsening process is controlled by diffusion in the matrix, so coarsening in A1 alloys is faster than that in A3 alloys at low volume fractions. However, high volume fractions, the particles are very close to each other and the diffusion process becomes less important, and the coarsening rate is controlled by the curvature. Thus the coarsening rate constants for A3 alloys are larger than those for A1 alloys at high volume fractions.

4. Summary

The microstructural evolution and coarsening kinetics of γ' precipitates in Ni–Al–Mo alloys were studied by phase-field simulations at length and time scales comparable to those used in experiments. With increasing Mo concentration, the lattice misfit between γ and γ' decreases, and the shape of the γ' particles changes from rectangular to circular. The cube of average particle size is observed to increase approximately linearly with time during the coarsening stage. The coarsening rate constant increases with the volume fraction of precipitates. With a low volume fraction, the increase in Mo concentration slows the coarsening process due to the reduced diffusivity. At high volume fractions, the coarsening rate can be accelerated by a higher Mo concentration which causes a larger curvature effect by changing the particle shape.

Acknowledgments

This work is funded by the National Science Foundation (NSF) through Grant DMR-0205232. Simulations were carried out on the LION clusters at the Pennsylvania State University supported in part by the NSF Grants (DMR-9983532, DMR-0122638, DMR-0710483 and DMR-0205232) and in part by the Materials Simulation Center and the Graduate Education and Research Services at the Pennsylvania State University. The authors also want to thank Dr. Michael G. Fahrmann for providing the original TEM images.

References

[1] Calderon HA, Kostorz G, Qu YY, Dorantes HJ, Cruz JJ, CabanasMoreno JG. Mat Sci Eng A Struct 1997;238:13–22.
[2] Qiu YY. J Mater Sci 1996;31:4311–9.
[3] Fahrmann M, Fratzl P, Paris O, Fahrmann E, Johnson WC. Acta Metall Mater 1995;43:1007–22.
[4] Conley JG, Fine ME, Weertman JR. Acta Metall 1989;37:1251–63.
[5] Wang Y, Khachaturyan AG. Acta Metall Mater 1995;43:1837–57.
[6] Vaithyanathan V, Chen LQ. Acta Mater 2002;50:4061–73.
[7] Zhu JZ, Wang T, Ardell AJ, Zhou SH, Liu ZK, Chen LQ. Acta Mater 2004;52:2837–45.
[8] Zhu JZ, Liu ZK, Vaithyanathan V, Chen LQ. Scripta Mater 2002;46:401–6.
[9] Cha PR, Yeon DH, Chung SH. Scripta Mater 2005;52:1241–5.
[10] Fan J, Greenwood M, Haataja M, Provatas N. Phys Rev E 2006;74:031602.
[11] Tan L, Zabaras N. J Comput Phys 2007;221:9–40.
[12] Luo W, Shen C, Wang Y. Acta Mater 2007;55:2579–86.
[13] Zhang W, Jin Y, Khachaturyan A. Acta Mater 2007;55:565–74.
[14] Simmons J, Wen Y, Shen C, Wang Y. Mat Sci Eng A Struct 2004;365:136–43.
[15] Granasy L, Borzsonyi T, Pusztai T. Phys Rev Lett 2002;88:206105.
[16] Artemev A, Jin Y, Khachaturyan A. Acta Mater 2001;49:1165–77.
[17] Zhang W, Jin Y, Khachaturyan A. Philos Mag 2007;87:1545–63.
[18] Li Y, Chen Z, Lu Y, Wang Y, Lai Q. Mater Lett 2007;61:974–8.
[19] Kitashima T, Wang J, Harada H. Intermetallics 2008;16:239–45.
[20] Wu K, Chang Y, Wang Y. Scripta Mater 2004;50:1145–50.
[21] Wen Y, Simmons J, Shen C, Woodward C, Wang Y. Acta Mater 2003;51:1123–32.
[22] Zhou N, Shen C, Mills M, Wang Y. Acta Mater 2007;55:5369–81.
[23] Boisse J, Lecoq N, Patte R, Zapolsky H. Acta Mater 2007;55:6151–8.
[24] Chen LQ. Ann Rev Mater Res 2002;32:113–40.
[25] Kim SG, Kim WT, Suzuki T. Phys Rev E 1999;60:7186–97.
[26] Zhou SH, Wang Y, Zhu JZ, Wang T, Chen LQ, MacKay RA, et al. Superalloys 2004:969–75.
[27] Tiaden J, Nestler B, Diepers HJ, Steinbach I. Physica D 1998;115:73–86.
[28] Khachaturyan AG. Theory of structural transformation in solids. New York: Wiley; 1983.
[29] T. Wang. Ph.D. Thesis. State College, PA: The Pennsylvania State University; 2006.
[30] West AW, Kirkwood DH. Scripta Metall 1976;10:681–6.
[31] Wang T, Zhu JZ, Mackay RA, Chen LQ, Liu ZK. Metall Mater Trans A 2004;35A:2313–21.
[32] Wang T, Chen LQ, Liu ZK. Mater Sci Eng A 2006;431:196–200.
[33] Staron P, Kampmann R. Acta Mater 2000;48:701–12.
[34] Zickler GA, Tian B, Lind C, Paris O. J Appl Crystallogr 2003;36:484–8.
[35] Prikhodko SV, Carnes JD, Isaak DG, Ardell AJ. Scripta Mater 1997;38:67–72.
[36] Prikhodko SV, Carnes JD, Isaak DG, Yang H, Ardell AJ. Metall Mater Trans A 1999;30:2403–8.
[37] Nabarro FRN. Metall Mater Trans A 1996;27:513–30.
[38] Fahrmann M, Hermann W, Fahrmann E, Boegli A, Pollock TM, Sockel HG. Mat Sci Eng A Struct 1999;260:212–21.
[39] Lifshitz IM, Slyozov VV. J Phys Chem Solids 1961;19:35–50.
[40] Wagner C. Z Elektrochem 1961;65:581–91.
[41] Furukawa H. Adv Phys 1985;34:703–50.
[42] Wen YH, Wang B, Simmons JP, Wang Y. Acta Mater 2006;54:2087–99.
[43] Speich G, Oriani R. T Metall Soc AIME 1965;233:623.
[44] Hoyt J. Acta Mater 1998;47:345–51.
[45] Kuehmann C, Voorhees P. Metall Mater Trans A 1996;27:937–43.
[46] Morral J, Purdy G. Scripta Metall Mater 1994;30:905–8.
[47] Umantsev A, Olson G. Scripta Metall Mater 1993;29:1135–40.
[48] Slezov V, Sagalovich V. J Phys Chem Solids 1977;38:943–8.
[49] Bhattacharyya S, Russell K. Metall Trans 1972;3:2195.
[50] Ardell AJ, Ozolins V. Nat Mater 2005;4:309–16.
[51] Seidman D, Sudbrack C, Yoon K. JOM 2006;58:34–9.
[52] Dwarapureddy A, Balikci E, Ibekwe S, Raman A. J Mater Sci 2008;43:1802–10.
[53] Sheng G, Du Q, Wang KG, Liu ZK, Chen LQ, in preparation..
[54] Asimow R. Acta Metall 1963;11:72–3.
[55] Ardell AJ. Acta Metall 1972;20:61.
[56] Brailsford AD, Wynblatt P. Acta Metall 1979;27:489–97.
[57] Davies CKL, Nash P, Stevens RN. Acta Metall 1980;28:179–89.

[58] Marqusee JA, Ross J. J Chem Phys 1984;80:536–43.
[59] Voorhees PW, Glicksman ME. Metall Trans A 1984;15:1081–8.
[60] Tokuyama M, Kawasaki K, Enomoto Y. Physica A 1986;134:323–38.
[61] Yao JH, Elder KR, Guo H, Grant M. Phys Rev B 1993;47:14110–25.
[62] Snyder VA, Akaiwa N, Alkemper J, Voorhees PW. Metall Mater Trans A 1999;30:2341–8.
[63] Kim DM, Ardell AJ. Scripta Mater 2000;43:381–4.